Applied Composite Materials (2023) 30:361–377
https://doi.org/10.1007/s10443-022-10086-5

Process Modeling for Strain Evolution during Autoclave Composite Cure

Sandeep Chava[1] · **Sirish Namilae**[1]

Received: 9 April 2022 / Accepted: 17 November 2022 / Published online: 6 December 2022

Abstract
Carbon fiber composites with epoxy matrix are widely used in many aerospace applications due to their high strength-to-weight ratio compared with commonly used metals. In addition to high mechanical performance, low dimensional tolerance and low defect count are requirements for primary aerospace structures in fuselage and wings. The continuous evolution of thermal and chemical strains and the resulting residual stresses during autoclave processing critically affect the dimensional stability and processing-induced defects in the composite structures. This research focuses on modeling the cure phenomenon inside an autoclave and presents a cure design technique to reduce the processing induced strains and stresses. The cure kinetics of the thermoset matrix of a carbon fiber prepreg is calculated through reaction kinetic equations parameterized using differential scanning calorimetry (DSC). A thermomechanical finite element model of autoclave composite processing incorporating cure kinetics is then developed. Processing induced deformations in a few four-ply layups are analyzed using this model and compared with prior experimental results. The effect of abrupt cooling operation in lowering the processing induced strains is investigated. The computational model accurately predicted the evolution of strains during cure and deformations post-cure. This approach can be applied to other thermoset matrix materials to predict and reduce processing-induced strains and residual stresses.

Keywords Cure monitoring · Reaction kinetics · Composite process modeling · Cure profile design · Finite element analysis

1 Introduction

While out-of-autoclave composite manufacturing is used for some applications [1, 2], autoclaves are commonly used for the manufacture of high-performance aerospace composite structures [3]. Typical autoclave processing steps employ high temperatures and pressures to enable curing as well as consolidation of the composite material. This process involves heat and mass transfer in a multi-component system with continually

✉ Sirish Namilae
Sirish.Namilae@erau.edu

[1] Department of Aerospace Engineering, Embry-Riddle Aeronautical University, Daytona Beach, FL 32114, USA

varying material properties due to polymerization reaction, subject to thermomechanical loads [3]. Discrepancies in processing parameters can lead to residual stresses and processing defects, therefore, a thorough understanding of the processing through experimentation and modeling is needed to mitigate processing defects and to improve the part quality.

Prior research on composite manufacturing process modeling includes two distinct aspects: modeling of heat transfer within the autoclave and thermochemical modeling of the composite cure process. Bohne et al. investigated the heat transfer inside an autoclave using lumped mass calorimeter measurements of heat transfer coefficients (HTC) and a fluid dynamics model [4]. They note that the process pressure and position inside an autoclave have a significant influence on the heat transfer while temperature and heating rates did not influence the HTC. Kluge et al. used computational fluid dynamics (CFD) simulations to predict the temperature distribution in composite parts in an autoclave using experimental input data [5]. Weber et al. developed a hybrid model using shift-factors, which incorporate flow effects by shifting a measured reference curve to a higher or lower HTC based on the orientation of the part surface with respect to convective flow within the autoclave [6].

The need for tool design incorporating spring-back and tool-part interaction in the composites industry has led to the development of manufacturing process simulation tools like COMPRO and ANSYS Composite Cure Simulation (ACCS) [7–9], which provide a virtual framework for process modeling [10, 11]. Several researchers have utilized these tools to analyze the processes involved in composite curing. Sreekantamurthy et al. developed cure process models to model the laminate cure responses with reference to the physics of the curing process using the cure simulation software COMPRO [8]. They compared the results of 2D and 3D models with reference to the formation of residual strains and warpage. They found that many cure process results from the simulation could be traced to the physical phenomenon occurring during cure such as cure kinetics, shrinkage, resin flow, and compaction. Twigg et al. conducted a parametric study of tool-part interaction induced warpage using COMPRO and compared the results with experimental data [12, 13]. They found that the elastic shear layer they used is unable to capture the shear stress that arises due to the sliding friction condition at the tool-part interface. The workaround they suggested to predict the warpage accurately is to adjust the shear layer stiffness. Fernlund et al. studied the effect of tooling material, tool-surface condition, and cure cycle on the spring-in behavior of composite laminates [14]. They used COMPRO to predict the flange spring-in after cure and compared it with experiments. Hubert et al. measured the compaction curve of unidirectional and quasi-isotropic AS4/3501–6 carbon epoxy prepregs [15]. They found that the force–displacement response from the simulations matched the experimental results.

ANSYS-based process modeling software ACCS is another modeling tool used to simulate the curing behavior of the resin and associated tool–part interaction. During the curing of thermosetting composites, the resin undergoes cross-linking resulting in gelation and vitrification which causes thermal and resin shrinkage. This behavior of the resin during the composite cure process can be captured by the ACCS material curing model. An approach to predict the final shape of the composite part using ACCS was developed by Patil et al. [16]. They applied ACCS chemical solver in the transient thermal module and simulation for the development of polymerization and glass transition temperature. They observed that the simulation results are 11% better than analytical calculations. Kumbhare et al. developed a design optimization method for composite structures that incorporates process-induced residual stresses and distortions [17].

Apart from these modeling studies, there have been several experimental studies focusing on processing induced deformations and residual stresses. Researchers have used methods such as layer removal [18], curvature measurements [19], Fiber Bragg Grating [20], and photoelasticity [21] to analyze processing induced deformations and to calculate residual stresses. Studies that measure the shape deformation are limited to post-cure measurements [22, 23]. In-situ approaches that use sensors like embedded strain gauges and fiber optics to measure the deformation introduces a foreign body into the laminate which changes the material properties [24]. Approaches for continuous evaluation of processing induced strains during cure are limited due to the experimental requirements of incorporating the monitoring setup inside an autoclave. In addition, there are very few studies that correlate process modeling and corresponding in-situ experimental data.

To address these limitations, the authors developed a novel in-situ experimental approach to measure dimensional changes in composite laminates during curing. This approach utilizes digital image correlation (DIC) to evaluate strains during autoclave processing [25]. The residual stresses for each ply were then calculated using the in-situ residual strain and temperature-dependent stiffness matrix of the composite panel. This experimental approach is effective for calculating the residual stresses throughout the cure for both symmetric and asymmetric layups. Results indicated that warpage developed in asymmetrical layups after processing. Higher residual stresses resulted in higher average warpage with the balanced unsymmetric [30/-30/60/-60] layup exhibiting an average warp of 1.46 mm.

The authors used this methodology to study a modified cure approach to reduce residual stresses during the cure [26]. The modified cure cycle consisted of controlled abrupt cooling as the matrix reached the gel point. Cooling was performed by relocating the sample from the autoclave to a walk-in freezer. The decrease in bonding temperatures due to the abrupt cooling resulted in lower residual stresses after vitrification and an increase in both the first-ply failure load and ultimate strength of both the symmetric and asymmetric layups. While these experimental approaches are effective in calculating and reducing the residual stresses, a combination of experiments with the corresponding computational model will be a useful tool for process design and optimization.

The focus of the current study is to develop a thermomechanical model for composite curing in an autoclave and use it in combination with recent experimental results to design a cure process that will reduce residual stresses. Differential scanning calorimetry (DSC) of the epoxy in the prepreg used in the experimental studies was utilized to parameterize the cure kinetics model. The cure kinetics model was combined with transient—thermal and structural finite element analysis using ANSYS–ACCS software. This method can calculate processing induced strains during composite curing under autoclave conditions. The model results were validated by comparison with in-situ experimental data and used for cure process design.

2 Experimental

2.1 Materials

Unidirectional carbon fiber prepreg procured from Fibre Glast Corporation contains 12 K tow raw material with manufacturer specified tensile modulus of 275.8×10^9 Pa and strength of 5.65×10^9 Pa. This prepreg is pre-impregnated with an epoxy resin system of

the density of 1.2×10^3 kg/m^3 and has a fabric areal weight of 139 gsm. Resin samples of weight 25×10^{-3} g to 35×10^{-3} g were extracted by scraping from the prepreg for cure kinetics. The manufacturer recommended curing temperature of the prepreg is 120 °C with a hold time of 1 h. This is the same material that is used in the in-situ process characterization experiments in our previous work [25].

2.2 Differential Scanning Calorimetry (DSC) Characterization

The energetics of chemical reactions in curing were obtained through Differential scanning calorimetry (DSC) using DSC-3 from Mettler Toledo. Resin samples extracted by scraping from the prepreg were placed and sealed in 40 µL aluminum crucibles. These crucibles were placed in DSC-3 with a constant 10 ml/min flow of nitrogen for characterization. The resin was heated from -25 °C to 250 °C with three different heating rates of 5 °C/min, 10 °C/min, and 15 °C/min in an inert nitrogen atmosphere. An empty crucible was used as a reference for all the tests. The heat flow data was obtained as a function of temperature and time using the area under the peak of the exotherm. This data was processed further to obtain the degree of cure (DOC) of the resin. DSC works on the basic assumption that the rate of the kinetic process ($d\alpha/dt$) is proportional to the measured heat flow (ϕ) as shown in Eq. (1) [27].

$$\frac{d\alpha}{dt} = \frac{\phi}{\Delta H} \tag{1}$$

where α is the DOC and ΔH is the enthalpy of the curing reaction.

3 Composite Cure Modeling

3.1 Reaction Kinetics

During the high temperature curing process, the epoxy matrix is involved in an exothermic reaction. The energy equation for the autoclave curing of thin structures with a non-linear internal heat generation term can be expressed as:

$$\rho C_p \frac{\partial\theta}{\partial t} - K_x \frac{\partial^2\theta}{\partial x^2} - K_y \frac{\partial^2\theta}{\partial y^2} = \rho_m H_m V_m \frac{\partial\alpha}{\partial t} \tag{2}$$

where θ is the temperature, ρ and C_p are the density and specific heat of the composite, K_x, and K_y are the thermal conductivities. ρ_m, H_m, V_m are the density, heat of reaction, and volume fraction of the epoxy matrix, α is the degree of cure. The densities and specific heats for the composite are typically calculated using the rule of mixtures. This Eq. (2) is discretized using transient thermal finite element analysis and combined with structural analysis in ANSYS ACCS and ACP modules. The model however requires the cure kinetics and energetics input parameterized using the aforementioned DSC analysis.

The right-hand side of Eq. (2) is governed by the kinetics of the polymerization reaction which is often phenomenologically expressed in terms of a temperature (θ) dependent reaction rate $K(\theta)$, and a kinetic model function $f(\alpha)$ as shown in Eq. (3) [28].

$$\frac{d\alpha}{dt} = K(\theta)f(\alpha) \tag{3}$$

The Arrhenius reaction rate is expressed as $K(\theta) = Ae^{-x}$, where A is the pre-exponential factor and $x = E_a/R\theta$ is the reduced activation energy, E_a is the activation energy and R is the universal gas constant. It is necessary to find both $K(\theta)$ and $f(\alpha)$ to understand the kinetics behind the cure phenomenon. The curing reaction of the epoxy resin in the prepreg was investigated by DSC at three different heating rates as shown in Fig. 1. The variation of the fractional conversion as a function of temperature for the epoxy resin can be seen in this Fig. 2.

The activation energy E_a can be determined by using the iso-conversional method using the logarithmic form of Eq. (3) as shown below [29]:

$$\ln\left(\frac{d\alpha}{dt}\right) = \ln(A.f(\alpha).e^{-\frac{E_a}{R\theta}}) \tag{4}$$

$$\ln\left(\frac{d\alpha}{dt}\right) = \frac{-E_a}{R}\left(\frac{1}{\theta}\right) + \ln(Af(\alpha)) \tag{5}$$

Activation energy can be determined from the slope of the plot $\ln(d\alpha/dt)$ versus $(1/\theta)$ for the same value of α.

The data from the DSC for the respective α is used in Eq. (5) to plot the Arrhenius equation for the cured resin samples as shown in Fig. 3. The slope of these straight lines gives the value of activation energy (E_a). The mean activation energy with the absolute mean error calculated from the slope is 70319 ± 4595 J/mol as shown in Table 1.

Two special functions $y(\alpha)$ and $z(\alpha)$ are utilized to determine the functional form of $f(\alpha)$ as discussed in [30]. These functions can easily be obtained through the experimental data using Eq. (6) and Eq. (7) respectively.

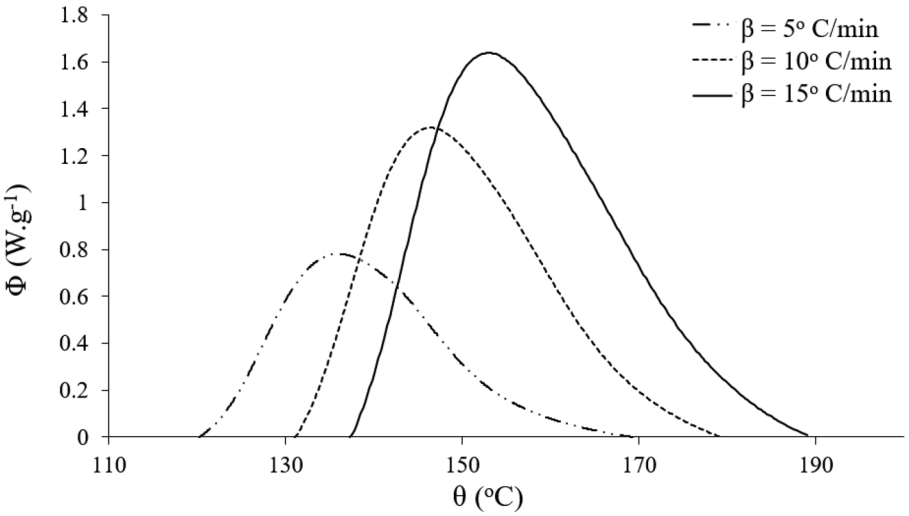

Fig. 1 Measured heat flow for different heating rates

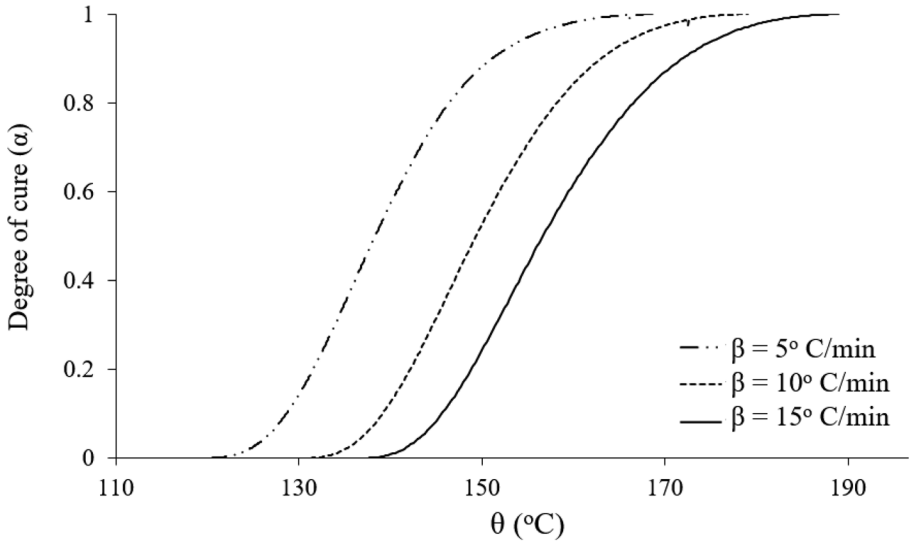

Fig. 2 Degree of cure for different heating rates

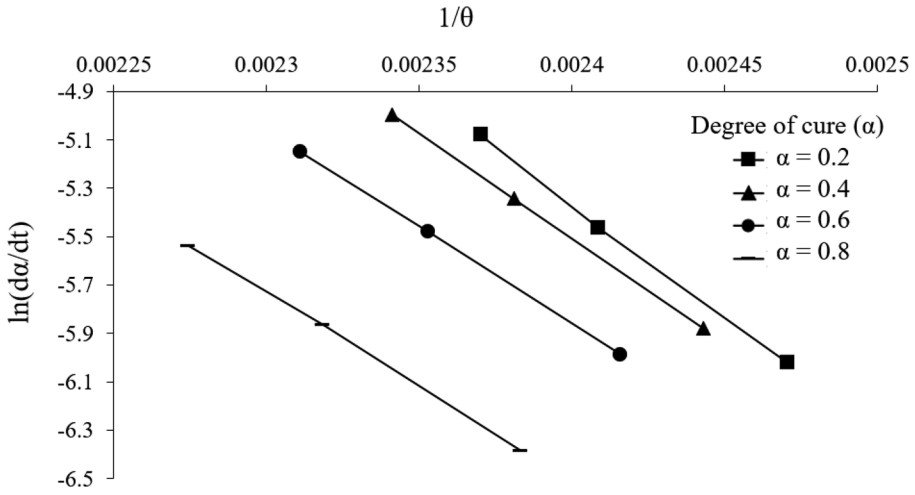

Fig. 3 $ln(d\alpha/dt)$ vs. $(1/\theta)$ for $\alpha = 0.2, 0.4, 0.6\&0.8$

Table 1 Activation energy calculated from the slope of Arrhenius plots

DOC (α)	E_a(J/mol)	Mean E_a (J/mol)
0.2	77676	70319
0.4	72152	
0.6	66621	
0.8	64826	

$$y(\alpha) = \left(\frac{d\alpha}{dt}\right)e^{x} \tag{6}$$

$$z(\alpha) = \pi(x)\left(\frac{d\alpha}{dt}\right)\left(\frac{\theta}{\beta}\right) \tag{7}$$

Here β is the heating rate (K/min) and $\pi(x)$ is the expression of the temperature integral which can be approximated using the 4th rational expression of Senum and Yang as in Eq. (8) [31].

$$\pi(x) = \frac{x^3 + 18x^2 + 88x + 96}{x^4 + 20x^3 + 120x^2 + 240x + 120} \tag{8}$$

Plotting the function $y(\alpha)$, normalizing within the (0,1) interval gives the shape of the function and as $y(\alpha)$ is proportional to the $f(\alpha)$ function, this plot is also the shape of the function $f(\alpha)$. The shapes and maximums of both these functions are used in determining the appropriate kinetic model function [32]. Some of the most frequently cited basic kinetic model functions are the Johnson–Mehl–Avrami model (JMA(n)) [33], 2D and 3D-reaction models (R2 & R3) [28], Ginstling-Broumshtein model (D4) [34], etc. The exponent n in the Johnson–Mehl–Avrami model depends on the mechanism of the nucleation-growth process and it remains constant for a given reaction [35].

Using the value of the activation energy and the kinetic model function, the value of the pre-exponential factor (A) is calculated using the following equation:

$$A = -\frac{\beta x_p}{\theta f'(\alpha_p)}e^{x_p} \tag{9}$$

where, $f'(\alpha_p)$ is the differential form of the kinetic model $[df(\alpha)/d\alpha]$, α_p is the conversion corresponding to the maximum on the DSC curve and p is the maximum of the DSC curve. The mean pre-exponential factor with absolute mean error considering all the heating rates is 7.5 ± 2.9 E8 as shown in Table 2. The normalized variation of functions $y(\alpha)$ and $z(\alpha)$ plot with the degree of cure can be seen in Fig. 4. Table 2 lists the values of the maxima of both the functions $y(\alpha)$ and $z(\alpha)$ at α_M and α_p^{∞} respectively and the peak of DSC α_p is the maximum of the measured heat flow obtained from DSC (Fig. 1).

From Table 2 it can be observed that the values of α_M are lower than the values of α_p and the value of α_p^{∞} is lower than 0.632. These values indicate that the curing process of the resin in the prepreg can be described using the two-parameter autocatalytic kinetic model also called Sestak-Berggren (SB) model shown in Eq. (10) [36].

$$f(\alpha) = \alpha^m(1-\alpha)^n \tag{10}$$

Here, m and n are the kinetic exponents. These exponents for the SB model are related to each other through the kinetic parameter ratio p which is $p = m/n$. The value of p is calculated using the maxima of function $y(\alpha)$ as $p = \alpha_M/(1-\alpha_M)$. The value of the kinetic parameter n for various heating rates is obtained by the slope of the linear dependence $\ln\left[\left(\frac{d\alpha}{dt}\right)e^{x}\right]$ versus $\ln[\alpha^p(1-\alpha)]$ [34]. The values of p, n, and m for all three heating rates can be seen in Table 2.

Table 2 Kinetic exponents calculated for various heating rates

Heating Rate β (°C/min)	α_M	α_p^∞	α_p	$\theta(K)$	P	x_p	N	Mean n	m	Mean m	A (s^{-1})	Mean A (s^{-1})
5	0.245	0.409	0.360	409	0.325	20.67	1.06	1.15	0.37	0.35	6.0E8	7.5E8
10	0.232	0.393	0.372	419	0.303	20.16	1.30		0.39		7.6E8	
15	0.214	0.377	0.358	425	0.273	19.85	1.08		0.29		8.8E8	

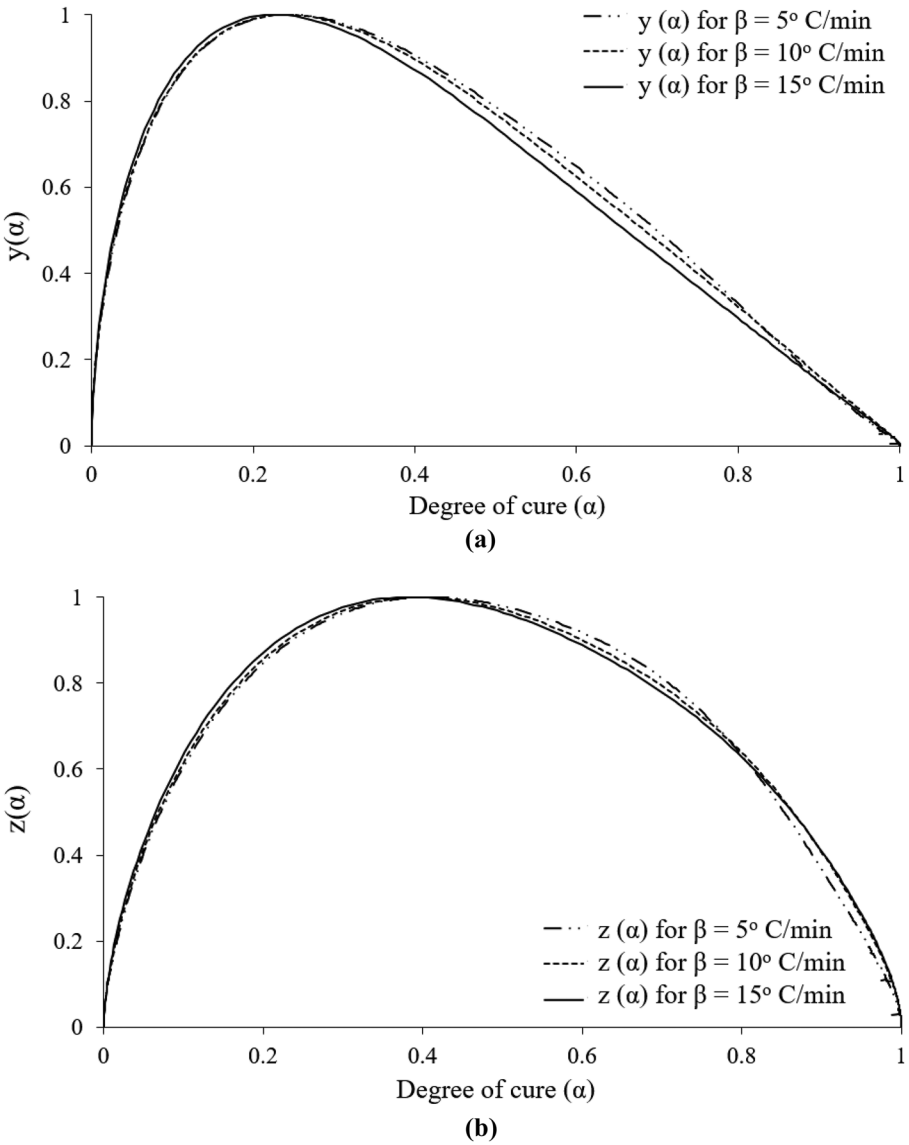

Fig. 4 (**a**) Variation of the functions with the degree of cure: $y(\alpha)$. (**b**) Variation of the functions with the degree of cure: $z(\alpha)$

4 Autoclave Process Modeling

The PDE in Eq. (2) can be discretized using finite element analysis (FEA) and combined with mechanical analysis to estimate the deformations and residual stresses during curing. In this study, a mechanical model from ANSYS Composite PrepPost (ACP) in combination with the transient thermal model from ANSYS Composite Cure Simulation (ACCS) was adopted for the process modeling. Solid brick elements were used

to model the four-ply composite laminates. Figure 5a shows a schematic sketch of the specimen along with the applied boundary conditions for the FEA simulation of the autoclave curing process. For this simulation, the temperature was varied based on the cure cycle, therefore the convective heat transfer boundary condition was considered for the FEA simulation. The dimensions and the layup of the composite correspond to the in-situ experimental setup from the authors' prior experimental work [25]. Uniform pressure was applied to simulate the vacuum bagging in the experiments. The experimentally determined heating rate and autoclave temperature profiles were incorporated as inputs to the finite element model. The temperature profile consists of three steps, a gradual temperature increase at a constant rate of 4.75 °C/min followed by isothermal heating, and post-cooling as shown in Fig. 5b. For simulating the entire curing process, thermomechanical material properties are needed for the analysis. The material state, glass transition temperature, and heat of reaction were obtained from the DSC of the samples. The cure kinetic equations were used to obtain the results such as Degree of Cure (DOC), activation energy, pre-exponential factor, '*m*', and '*n*'. The rest of the material properties associated with fiber such as Young's modulus, Poisson's ratio, and shear modulus were provided by the prepreg manufacturer. The in-situ strain data as a function of temperature was used in calculating the coefficient of thermal expansion (CTE) [37, 38].

A convergence study on the ACCS model was carried out to determine an appropriate mesh density. The element size of 5 mm was selected by performing an adaptive mesh refinement study with mesh sizes ranging from 20 to 2 mm.

4.1 Cure Simulation Results

The kinetic parameters and thermal boundary conditions were imported into the ACP/ACCS FE model for cure modeling. The strain on the top ply was extracted and compared with the experimental data from previous studies [25]. The strain evolution for [30/-30/60/-60] laminate is shown in Fig. 6. As shown in this figure, the predicted strain by the model matches well with the experimental data. This result indicates that the model is in good agreement with the experimental results.

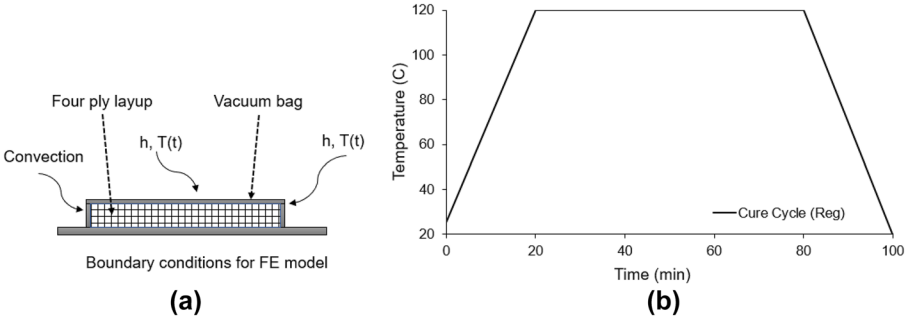

Fig. 5 Temperature profile incorporated into the finite element model

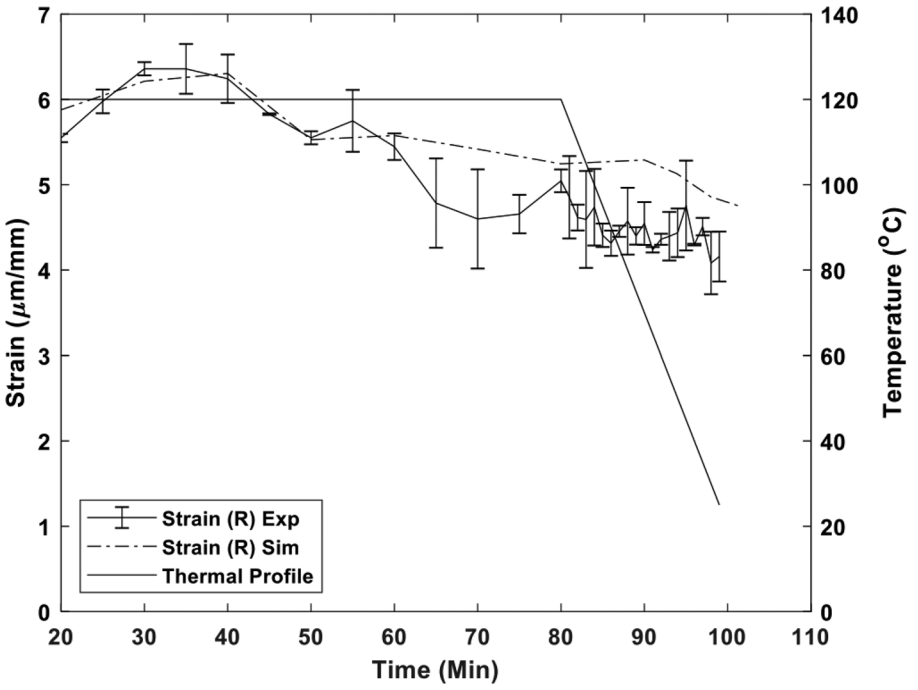

Fig. 6 In-situ experimental vs simulation strain for balanced [30/-30/60/-60] laminate

4.2 Cure Profile Design

After successfully setting up the cure simulation model, the next step is to design the cure profile to reduce the cure-induced strains. It is known from the literature that abruptly interrupting the curing process reduces the bonding temperatures of the fiber and matrix, and this low-temperature bonding results in lower cure-induced residual stresses [39–41]. The cure interruption point is the primary process design variable that plays a key role in optimizing the cure profile and reducing residual stresses. For the matrix considered in this simulation, the gel point is at 120 °C, and choosing the interruption point before the gel point is ineffective as the resin cross-linking would not start before the gel point. Similarly, interrupting the cure, post vitrification will not be effective either as the matrix is almost completely cured after this point. Therefore, three different points were programmed in the simulation to interrupt the cure as shown in Fig. 7.

The first interruption point was chosen to be the gel point of the resin at 20 min. This is the preferred interruption point according to the experiments. The second and third points were chosen to be at 40 min and 60 min into the cure as interrupted cure points 1 and 2 (IC1 and IC2) respectively. These three cure profiles were programmed into the model for [30/-30/60/-60] layup. The strain evolution for the regular cure profile and three modified cure profiles were extracted from the simulation and plotted as shown in Fig. 8. It can be observed that the strain at the end of the cure for the cure profile interrupted at gel point was lower than the regular cure profile. On the other hand, the strain at the end of the cure for IC1 and IC2 was higher than the regular strain. These results agree with the literature

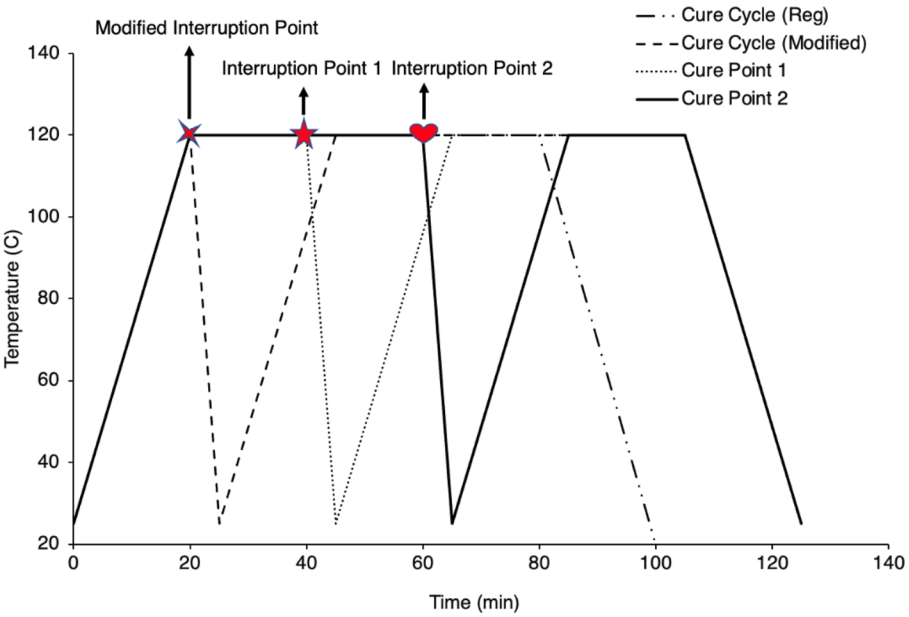

Fig. 7 Modified cure profiles with three new cure interruption points

that interrupting the cure at gel point is effective in reducing the processing induced strains thereby reducing residual stresses [39–41]. Essentially, interrupting the cure at the gel point and abruptly cooling the sample decreases resin diffusion.

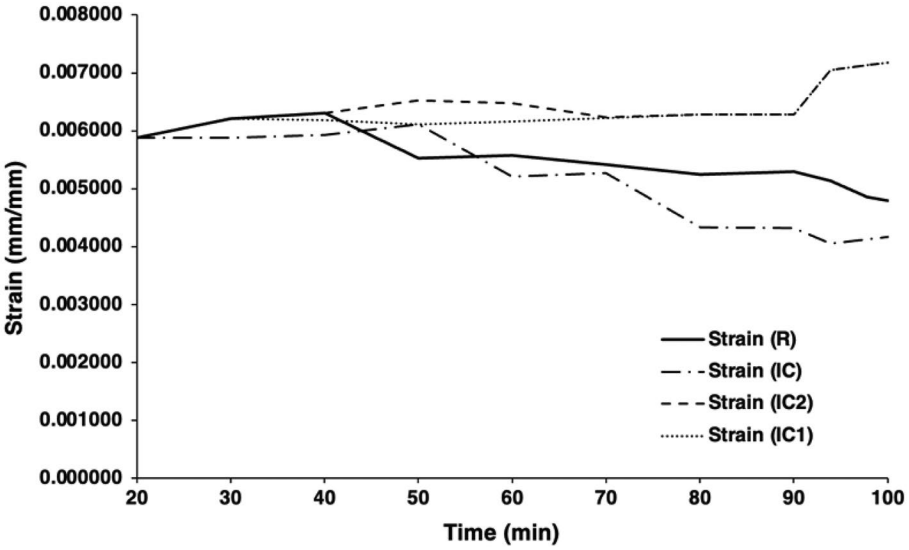

Fig. 8 Strain evolution for regular and the three interrupted cure profiles

On the other hand, the chemical reaction continues because of the exothermal reaction heat during the cure interruption. In addition, experiments show that an abrupt-cooling operation after gelation could efficiently dissipate the strain generated by the laminate thermal contraction owing to the viscoelastic behavior of the resin [42]. It has been reported that this reduction in strain decreases the bonding temperatures between adjacent plies thereby reducing the residual stresses. A recent experimental study by the authors using an in-situ DIC approach and thermal camera confirmed these observations [26]. Cure interruption after reaching the gel-point resulted in lower strain during and after curing, compared to the default case because of lower temperature curing. This resulted in decreased residual stresses and increased strength [26].

The optimized cure profile with the gel point as the cure interruption point was used to analyze the strain evolution for the layups considered in this study. The simulation prediction for balanced [30/-30/60/-60] layup was compared against experimental data in Fig. 9. It can be observed that the predicted strain for this layup matches well with experimental interrupted cure strains. The finite element model was also used to analyze the strain evolution for symmetric $[0/45]_s$ and angle-ply [45/-45/45/-45] laminates and compared with the experimental data. For better visualization of the results, the difference in strain (Δ) between regular cure and interrupted cure for the experimental data is compared with the difference in strains (Δ) from the FE model for these three laminates in Fig. 10. The solid lines in this figure represent the average experimental delta and the broken lines represent the delta of the FE model. The FE model also predicts the final deformed shape of the laminate. Figure 11 shows the experimental deformed [30/-30/60/-60] laminate compared against the FE model. The total warp including cup, bow,

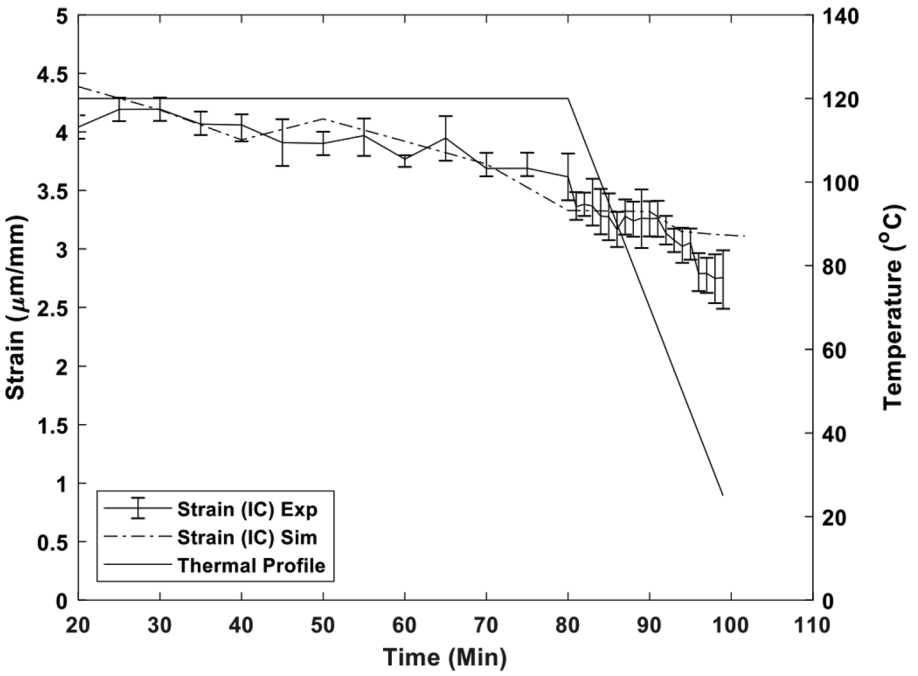

Fig. 9 Strain evolution comparison for interrupted cure profile for [30/-30/60/-60]

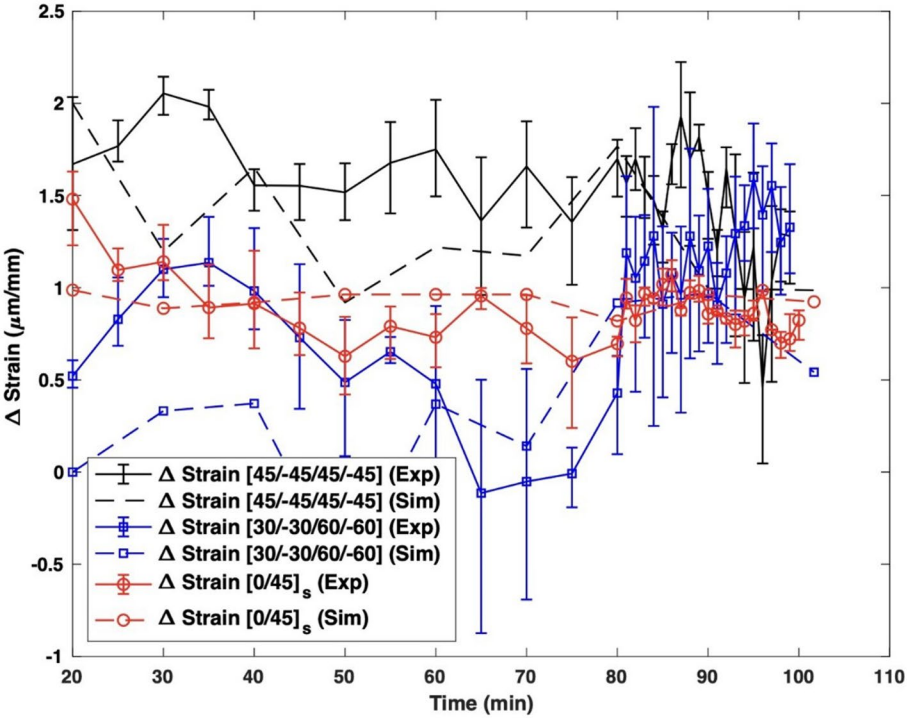

Fig. 10 Strain difference between a regular and optimized cure for [45/-45/45/-45] and $[0/45]_s$ layups

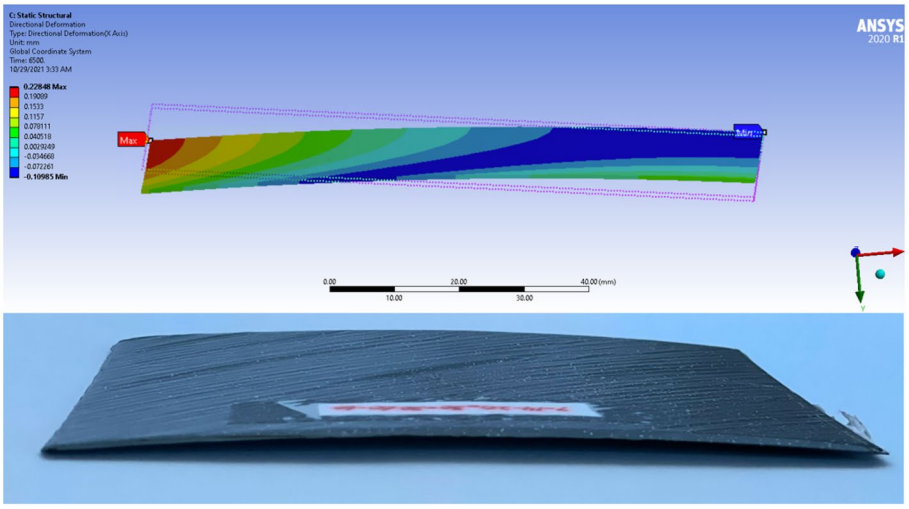

Fig. 11 After cure deformed shape comparison of [30/-30/60/-60] laminate

and twist warp is 1.46 mm for the experimental setup and 1.77 mm for the FE model. Note that the layups consist of four plys which results in a thin structure. The DIC experiments in Ref [25] consider surface ply strains to be same as the interior strains because of the low thickness. This is not a valid assumption for thicker structures and through thickness thermal gradients would need to be considered. While the modeling approach could still be applicable for thicker structures, the current experimentally validated results are limited to thin composite structures.

These results show that the FE model developed using ACP and ACCS is effective in predicting the strain during cure for both regular and optimized cures. It is apparent that interrupting the cure profile at the gel point of the resin is effective in reducing the processing strains which in turn reduces residual stresses. The results support the choice of gel point as the point for interrupting the cure for abruptly cooling to reduce the bonding temperature. This approach can be used to design cure cycles for any matrix material to reduce cure-induced residual stresses. Reduction in residual stresses decreases manufacturing defects and increases the ultimate strength of the cured parts. In future studies, the validated modeling approach described in this investigation can be used in an optimization framework to evaluate the optimal cure cycles for different objectives such as minimizing distortion, residual stresses, or cure time.

5 Conclusion

In this paper, a thermomechanical cure model was developed using ACP and ACCS to model the composite cure process, and the results of the model are compared with the experimental data from prior research. The resin reaction kinetics and related material properties were evaluated using DSC experimentation. A formulation was developed to calculate the activation energy and cure kinetics parameters, which were used as input to the FE model. In-situ cure strains were characterized through the mechanical model using ACP and transient thermal model using ACCS with predefined boundary conditions was used to simulate the cure phenomena inside an autoclave. A comparison of the strain between the experimental and simulation data indicated that the computational model accurately predicted the strain evolution and the final deformed shape of the laminate. This approach was used for cure profile design. The cure simulation was modified using multiple abrupt cooling points and the results suggested that the gel point is the optimum point to interrupt the cure for reducing processing induced strains and residual stresses. The modeling approaches developed in this study can be applied to any matrix material and can be used for process design to reduce residual stresses.

Acknowledgements The authors would like to acknowledge Dr. Sandra Boetcher for her support in using the DSC machine.

Funding This work was funded by NSF AM contract number 2001038.

Data Availability The data will be made available on request.

Declarations

Conflicts of Interest/Competing Interests The authors have no conflicts of interests to declare.

References

1. Khan, Z.I., Mohamad, Z., Rahmat, A.R., Habib, U.: Synthesis and Characterization of Composite Materials with Enhanced Thermo-Mechanical Properties for Unmanned Aerial Vehicles (Uavs) and Aerospace Technologies. Pertanika J. Sci. Technol. **29**, 3 (2021)
2. Khan, Z.I., Arsad, A., Mohamad, Z., Habib, U., Zaini, M.A.A.: Comparative study on the enhancement of thermo-mechanical properties of carbon fiber and glass fiber reinforced epoxy composites. Mater. Today Proc. **39**, 956–958 (2021)
3. Hubert, P., Fernlund, G., Poursartip, A.: Autoclave processing for composites. In: Manufacturing techniques for polymer matrix composites (PMCs), pp. 414–434. Woodhead Publishing (2012). https://doi.org/10.1533/9780857096258.3.414
4. Bohne, T., Frerich, T., Jendrny, J., Jürgens, J.-P., Ploshikhin, V.: Simulation and validation of air flow and heat transfer in an autoclave process for definition of thermal boundary conditions during curing of composite parts. J. Compos. Mater. **52**, 1677–1687 (2018)
5. Kluge, J.N.E., Lundström, T.S., Westerberg, L.-G., Nyman, T.: Modelling heat transfer inside an autoclave: effect of radiation. J. Reinf. Plast. Compos. **35**, 1126–1142 (2016)
6. Weber, T.A., Arent, J.-C., Steffens, L., Balvers, J.M., Duhovic, M.: Thermal optimization of composite autoclave molds using the shift factor approach for boundary condition estimation. J. Compos. Mater. **51**, 1753–1767 (2017)
7. Convergent Manufacturing Technologies: COMPRO Simulation Software. https://www.convergent.ca/products/compro-simulation-software
8. Sreekantamurthy, T., Hudson, T.B., Hou, T.-H., Grimsley, B.W.: Composite cure process modeling and simulations using COMPRO® and validation of residual strains using fiber optics sensors. In: American Society for Composites: Thirty-First Technical Conference, Williamsburg, VA (2016)
9. Patil, A.S., Moheimani, R., Dalir, H.: Thermomechanical analysis of composite plates curing process using ANSYS composite cure simulation. Therm. Sci. Eng. Prog. **14**, 100419 (2019)
10. Abdelal, G.F., Robotham, A., Cantwell, W.: Autoclave cure simulation of composite structures applying implicit and explicit FE techniques. Int. J. Mech. Mater. Des. **9**, 55–63 (2013). https://doi.org/10.1007/s10999-012-9205-7
11. Bedayat, H., Forghani, A., Hickmott, C., Palmieri, F., Grimsley, B., Coxon, B., Fernlund, G., Poursartip, A.: Numerical and experimental study of local resin pressure for the manufacturing of composite structures and their effect on porosity. In: SAMPE 2018 Technical Conference and Exhibition, Long Beach, CA (2018)
12 Twigg, G., Poursartip, A., Fernlund, G.: Tool–part interaction in composites processing. Part I: experimental investigation and analytical model. Compos. Part A Appl. Sci. Manuf. **35**, 121–133 (2004)
13 Twigg, G., Poursartip, A., Fernlund, G.: Tool–part interaction in composites processing. Part II: numerical modelling. Compos. Part A Appl. Sci. Manuf. **35**, 135–141 (2004)
14. Fernlund, G., Poursartip, A.: The effect of tooling material, cure cycle, and tool surface finish on spring-in of autoclave processed curved composite parts. In: Proceedings of ICCM. pp. 5–9 (1999). https://www.iccm-central.org/Proceedings/ICCM12proceedings/site/papers/pap690.pdf
15. Hubert, P., Poursartip, A.: A method for the direct measurement of the fibre bed compaction curve of composite prepregs. Compos. Part A Appl. Sci. Manuf. **32**, 179–187 (2001)
16. Patil, A., Moheimani, R., Shakhfeh, T., Dalir, H.: Analysis of Spring-in for Composite Plates Using ANSYS Composite Cure Simulation. Presented at the (2019)
17. Kumbhare, N., Moheimani, R., Dalir, H.: Analysis of composite structures in curing process for shape deformations and shear stress: basis for advanced optimization. J. Compos. Sci. **5**, 63 (2021)
18. Ersoy, N., Vardar, Ö.: Measurement of residual stresses in layered composites by compliance method. J. Compos. Mater. **34**, 575–598 (2000). https://doi.org/10.1106/KK4W-0E04-ACU5-CKCN
19. Wisnom, M.R., Gigliotti, M., Ersoy, N., Campbell, M., Potter, K.D.: Mechanisms generating residual stresses and distortion during manufacture of polymer-matrix composite structures. Compos. Part A Appl. Sci. Manuf. **37**, 522–529 (2006). https://doi.org/10.1016/j.compositesa.2005.05.019
20. Hannusch, S., Stockmann, M., Ihlemann, J.: Experimental method for residual stress analysis with fibre bragg grating sensors. Mater. Today Proc. **3**, 979–982 (2016). https://doi.org/10.1016/j.matpr.2016.03.032
21. Pawlak, A., Zinck, P., Galeski, A., Gerard, J.F.: Photoelastic studies of residual stresses around fillers embedded in an epoxy matrix. In: Macromolecular Symposia. pp. 197–210. Wiley Online Library (2001). https://doi.org/10.1002/1521-3900(200105)169:1
22. Tavakol, B., Roozbehjavan, P., Ahmed, A., Das, R., Joven, R., Koushyar, H., Rodriguez, A., Minaie, B.: Prediction of residual stresses and distortion in carbon fiber-epoxy composite parts due to curing process using finite element analysis. J. Appl. Polym. Sci. **128**, 941–950 (2013). https://doi.org/10.1002/app.38075

23. Benedikt, B., Rupnowski, P., Kumosa, L., Sutter, J.K., Predecki, P.K., Kumosa, M.: Determination of interlaminar residual thermal stresses in a woven 8HS graphite/PMR-15 composite using X-ray diffraction measurements. Mech. Adv. Mater. Struct. **9**, 375–394 (2002). https://doi.org/10.1080/15376490290097026
24. Bhat, M.R.: Non-destructive evaluation of defects and damage in composite materials and structures. J Indian Inst Sci **93**(4), 751–766 (2013)
25. Chava, S., Namilae, S.: Continuous evolution of processing induced residual stresses in composites: An in-situ approach. Compos. Part A Appl. Sci. Manuf. **145**, 106368 (2021). https://doi.org/10.1016/j.compositesa.2021.106368
26. Chava, S., Namilae, S., Al-Haik, M.: Residual stress reduction during composite manufacturing through cure modification: In situ analysis. J. Compos. Mater. **56**, 975–988 (2022)
27. Roşu, D., Caşcaval, C.N., Mustață, F., Ciobanu, C.: Cure kinetics of epoxy resins studied by non-isothermal DSC data. Thermochim. Acta. **383**, 119–127 (2002)
28. Yousefi, A., Lafleur, P.G., Gauvin, R.: Kinetic studies of thermoset cure reactions: a review. Polym. Compos. **18**, 157–168 (1997)
29. Vyazovkin, S.: Advanced isoconversional method. J. Therm. Anal. Calorim. **49**, 1493–1499 (1997)
30. Málek, J.: The kinetic analysis of non-isothermal data. Thermochim. Acta. **200**, 257–269 (1992)
31. Pérez-Maqueda, L.A., Criado, J.M.: The accuracy of Senum and Yang's approximations to the Arrhenius integral. J. Therm. Anal. Calorim. **60**, 909–915 (2000)
32 Koga, N., Malek, J.: Accommodation of the actual solid-state process in the kinetic model function. Part 2. Applicability of the empirical kinetic model function to diffusion-controlled reactions. Thermochim. Acta. **282**, 69–80 (1996)
33. Fanfoni, M., Tomellini, M.: The johnson-mehl-avrami-kohnogorov model: a brief review. Nuovo Cim. D. **20**, 1171–1182 (1998)
34. Ginstling, A.M., Brounshtein, B.I.: Concerning the diffusion kinetics of reactions in spherical particles. J. Appl. Chem. USSR. **23**, 1327–1338 (1950)
35. Arshad, M.A., Maaroufi, A.: Relationship between Johnson–Mehl–Avrami and Šesták-Berggren models in the kinetics of crystallization in amorphous materials. J. Non. Cryst. Solids. **413**, 53–58 (2015)
36. Montserrat, S., Málek, J.: A kinetic analysis of the curing reaction of an epoxy resin. Thermochim. Acta. **228**, 47–60 (1993)
37. Schulz, W.A., Myers, D.G., Singer, T.N., Ifju, P.G., Haftka, R.T.: Determination of residual stress and thermal history for IM7/977-2 composite laminates. Compos. Sci. Technol. **65**, 2014–2024 (2005)
38. Kim, H.S., Park, S.W., Lee, D.G.: Smart cure cycle with cooling and reheating for co-cure bonded steel/carbon epoxy composite hybrid structures for reducing thermal residual stress. Compos. Part A Appl. Sci. Manuf. **37**, 1708–1721 (2006). https://doi.org/10.1016/j.compositesa.2005.09.015
39. Weitsman, Y.: Residual thermal stresses due to cool-down of epoxy-resin composites. J. Appl. Mech. Trans. ASME. **46**, 563–567 (1979). https://doi.org/10.1115/1.3424606
40. Kim, J.S., Lee, D.G.: Development of an autoclave cure cycle with cooling and reheating steps for thick thermoset composite laminates. J. Compos. Mater. **31**, 2264–2282 (1997)
41. Kim, H.S., Yoo, S.H., Chang, S.H.: In situ monitoring of the strain evolution and curing reaction of composite laminates to reduce the thermal residual stress using FBG sensor and dielectrometry. Compos. Part B Eng. **44**, 446–452 (2013). https://doi.org/10.1016/j.compositesb.2012.04.021
42. Yinnon, H., Uhlmann, D.R.: Applications of thermoanalytical techniques to the study of crystallization kinetics in glass-forming liquids, part I: theory. J. Non. Cryst. Solids. **54**, 253–275 (1983)